Colloids and Surfaces A 572 (2019) 97–106

Contents lists available at ScienceDirect

Colloids and Surfaces A

journal homepage: www.elsevier.com/locate/colsurfa

Sessile droplets shape response to complex body forces

Inmaculada Ríos-López[a], Maria Petala[b], Margaritis Kostoglou[a], Thodoris D. Karapantsios[a,*]

[a] Department of Chemical Technology & Industrial Chemistry, Faculty of Chemistry, Aristotle University of Thessaloniki, 541 24, Thessaloniki, Greece
[b] Department of Civil Engineering, Faculty of Engineering, Aristotle University of Thessaloniki, 54124, Thessaloniki, Greece

GRAPHICAL ABSTRACT

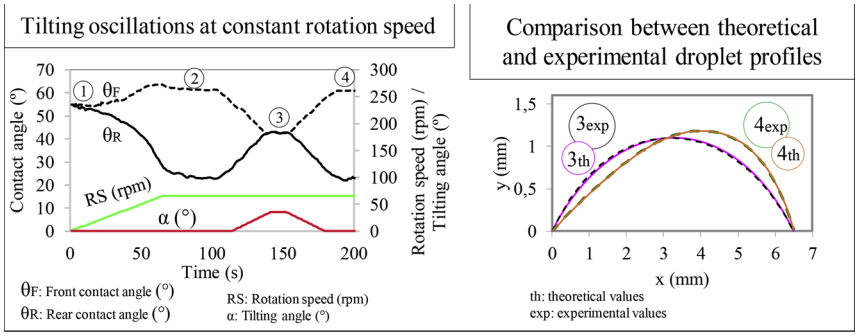

ARTICLE INFO

Keywords:
Forced wetting
Tangential force
Droplet shape
Contact angle
Young-Laplace equation

ABSTRACT

The majority of studies on forced wetting of sessile droplets refers to application of a steadily increasing normal or tangential force or to a specific combination of these forces arising from tilting the substrate. The above constitute well-defined test conditions but are not representative of what is encountered in most industrial applications. To approach realistic industrial conditions and so also expand existing wetting theories, an evaluation of droplet shape deformation under the influence of a complicated evolution of body forces, is performed herein. To this aim, two sets of experiments are carried out in *Kerberos* device creating force fields by combination of gravitational and centrifugal forces: i) by oscillations of the tilting angle at constant rotation speed and ii) by alternating small step-increases of the rotation speed and the tilting angle, one after the other, so as to trail the symmetric side profile (SSP) curve of a droplet. The latter is done in three or six steps following two different paths: increasing first either the rotation speed or the tilting angle. The aim of the experiments is, on one hand, to explore droplet deformation under cycles of increasing/decreasing tangential forces and, on the other hand, to analyze the effect of residual tangential forces on droplet shape. Several features related to the droplet shape evolution are investigated such as contact angles, side and top contour profiles and droplet 3-dimensional shape. The resulting droplet profiles are analyzed using numerical solutions of the Young-Laplace equation. It is found that the 3-dimensional Young Laplace equation can describe very accurately the experimental profiles.

1. Introduction

Wetting science is of crucial importance in countless natural [1,2], and industrial processes [3–5]. Its relevance has led to a vast scientific effort to elucidate the intricate mechanisms present in wetting phenomena [6]. Wetting arises from the interaction between liquids and

* Corresponding author.
E-mail address: karapant@chem.auth.gr (T.D. Karapantsios).

https://doi.org/10.1016/j.colsurfa.2019.03.096
Received 30 November 2018; Received in revised form 27 March 2019; Accepted 31 March 2019
Available online 03 April 2019

solids when they are in contact and, despite its ostensible simplicity, these processes are highly complex as they are governed by i) viscous, gravitational, capillary and inertial forces; ii) properties of the solid such as roughness, flatness, porosity and heterogeneities, and iii) properties of the liquid such as surface tension and viscosity [7]. When a liquid droplet is carefully deposited onto a solid surface, the liquid-solid contact line moves towards the thermodynamic equilibrium determined by the intrinsic properties of the liquid/solid system. This is a *spontaneous wetting* process dominated by forces that arise from liquid-solid interactions alone. Nevertheless, external forces may be applied to drive the system beyond the thermodynamic equilibrium in the so-called *forced wetting* processes [8]. In this case the movement of the liquid-solid contact line is triggered by externally imposed mechanical, electrical [9] or hydrodynamic [10] forces. The wetting process is then promoted by the dynamic balance between the system natural tendency to equilibrium and the external force leading the system away from it [8].

This work focuses on forced wetting experiments in which droplets are submitted to external mechanical forces such as gravitational, centrifugal and their combination. First experiments manipulating gravitational forces were performed in the early 90 s by means of the Tilted plate technique [11]. Although this technique is still in use due to its simplicity, it has important drawbacks because the maximum force that can be applied to the droplet is limited by its own weight, thus this method is not suitable to test small droplets [12]. Moreover, every tilting angle of the plate yields a pair of normal/tangential forces whose components cannot be adjusted independently. The use of centrifugal forces to study wetting emerged from the necessity to test small droplets [13]. By placing the solid substrate on a rotating disk, researchers managed to investigate a broader range of droplet's sizes. However, only tangential (i.e. lateral) forces can be customized if just the substrate rotation speed is adjusted.

The last decade, a new technique has been developed combining gravitational and centrifugal forces with the aim of controlling independently both, normal and tangential, components of the applied force. The new technique calls for simultaneous, but separate, adjustment of the rotation speed and tilting angle of the droplet's substrate. A pioneering device implementing this technique was designed by Karapantsios et al. [14] with the technological aim of characterizing the adhesiveness of tomato pulp pastes, with different solids and moisture content, on solid substrates. Shortly later, another investigation was conducted with this technique for determining the lateral adhesion of droplets to solid substrates [15]. Nevertheless, many industrial applications require data on the response of droplets exposed to more complicated external body force scenarios than the single increasing of tangential or normal force. For example, during wetting of non-flat or curved surfaces, the impact of liquid droplets on a surface generates a spectrum of droplets with different (non-axisymmetric) shapes. The contact area between the droplet and the surface will not be circular and this fact will have an effect on the spreading/sliding behavior of those droplets. Recently our research team has designed and constructed a new device (*Kerberos*) [16] that, besides an independent manipulation of tangential and normal forces, it also allows three-dimensional recording of wetting phenomena [17,18]. Using combination of rotation and tilting, *Kerberos* can generate droplets with non-axisymmetric shapes providing the means for examining their wetting behavior. So, the scope of this work is to use *Kerberos* to test droplet shape evolution under some complex body force scenarios. In addition, the resulting data are assessed in the context of corresponding theories.

The structure of the work is the following: At first, the employed materials and experimental procedures are described, being followed by the presentation and discussion of results. The final section includes the development of a mathematical model for describing droplet shapes and its comparison with experiments.

2. Materials and methods

All experiments are performed in *Kerberos*, a device designed for the study of forced wetting in which the combination of rotation and tilting allows independent and accurate control of the tangential and normal forces acting on a droplet placed on top of a solid substrate. Moreover, *Kerberos* offers recording all relevant phenomena (e.g. deformation of the liquid interface, spreading and sliding of the droplet along the substrate) by means of three Wi-Fi cameras viewing the droplet simultaneously from an X-Y-Z orthogonal perspective (top, side and back). The acquired video streams are processed with a custom software to extract relevant wetting properties (i.e. contact angles, droplet length, height, width, etc.) from side and top-view images. The droplet contour from the side-view is fitted with a 4th degree polynomial equation using the 30% of the total contour points in the fitting in order to obtain contact angle values at both droplet edges. Nevertheless, these parameters can be adjusted in the software to tailor different droplet shapes, if required. Thereafter, the combination of side and top-view images enables a 3-dimensional reconstruction of the droplet body. Further operational and technical details of *Kerberos* can be found in [16] whereas the image processing technique in 2D and 3D is described in [17].

The system under study consists of common microscope glass slides acting as the solid substrate and ultrapure water (ultrapure water, Direct-Q, Merck Millipore) acting as the liquid. Glass slides are cleaned before each experimental run by immersion in a 60% solution of nitric acid for two hours. Afterwards, the glass slides are rinsed with deionized water and dried in a stream of filtered air. A low concentration of dye (0.5 g/L of brilliant blue dye, Hina Dye Chem Industries) is dissolved in the ultrapure water to enhance the image analysis by means of increasing images contrast. Possible deviations arising from the addition of dye are evaluated by comparing (i) the surface tension of the dye-water solution with that of pure water and (ii) the dynamic contact angles of a droplet with the substrate with and without the dye. Surface tension measurements are performed using the Wilhelmy plate (TE2, LAUDA) and the maximum bubble pressure (BPA-1SX, Sinterface) techniques providing identical results with and without the dye. Dynamic contact angles of dye-water and pure water droplets over glass are obtained using the conventional injection/withdrawal method and *Kerberos* providing again identical results with and without the dye. These comparisons confirm that interfacial properties of both the liquid and solid are essentially not affected by the presence of low concentration of dye. Droplets are deposited on top of the substrate with a syringe (1750 LTN SYR, Hamilton) coupled with a repeating dispenser (PB600-1, Hamilton) that supplies 10 μL of liquid every time a button is pushed. All experiments are executed in the rotating/tilting test head of *Kerberos* which is enclosed inside a glovebox chamber regulated at 25 ± 2 °C and relative humidity of 50 ± 5%.

Experiments are performed to examine droplets behavior under two different scenarios of applied forces. The first scenario refers to oscillating the tilting angle of the substrate between a maximum value and zero value (horizontal position) while keeping the rotation speed constant. The scope is to periodically increase and decrease the tangential force applied to the droplet accompanied by a small variation of the normal force. The second scenario refers to alternating small steps of increasing the rotation speed and the tilting angle, one at a time, in order to trail the nominal rotation speed-tilting angle trajectory for achieving a droplet symmetric side profile (denoted as SSP curve). The SSP curve is approached in either three or six steps. The scope is to register the droplet deformation in the presence of residual tangential forces different from those that ensure symmetry. The term symmetry here designates only that the front and rear contact angles are the same and not that there is exact mirror image symmetry between the left and right side of the droplet side profile.

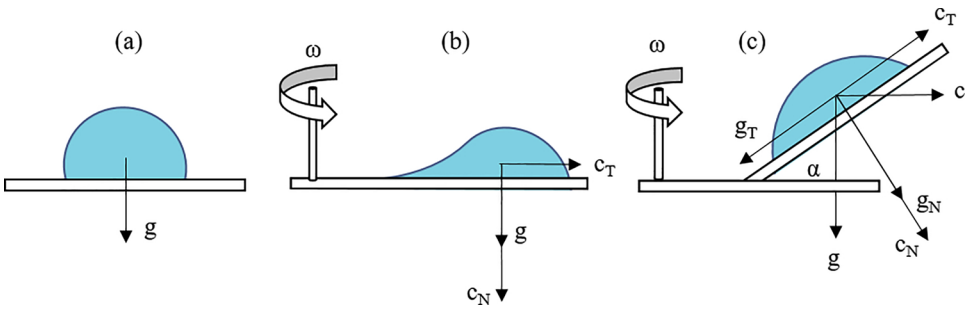

Fig. 1. Forces acting on a droplet over a) horizontal static substrate, b) horizontal substrate rotating at a constant rotation speed, *RS*, where droplet spreading (right edge movement) is noticed, c) tilted substrate at α angle -while rotating at the same speed, *RS*, as in (b)- so as the droplet remains symmetrical from a side perspective.

2.1. Tilting oscillations procedure

The first group of experiments is performed for three different droplet volumes (10, 20 and 30 μL). A droplet is initially placed on a horizontal substrate, thus its shape is axisymmetric (**Fig. 1a**). Then, the centrifugal force is gradually increased by increasing the rotation speed (*RS*) at 1 rpm/s until some degree of droplet spreading is noticed. Spreading is defined here as the movement of the droplet's front edge while the rear edge remains pinned to the surface. As a consequence of spreading, the droplet elongates in the direction of the tangential component of the centrifugal force (c_T) acquiring a non-axisymmetric configuration. This configuration can be maintained by keeping the applied force constant (**Fig. 1b**). Having the non-axisymmetric droplet rotating at constant speed, the tilting angle α is then increased at a rate of 1.3°/s in a way such that the tangential component of gravitational force (g_T) opposes the tangential component of the centrifugal force (c_T) (Fig. 1c). Upon increasing the tilting angle, an evolving combination of centrifugal and gravitational forces is applied to the droplet. Tilting advances up to an angle where the droplet reaches a side profile with equal front and rear contact angles. Thereafter, the substrate is returned back to the horizontal position, where the centrifugal force has only tangential component. Three oscillations are performed between the horizontal **(b)** and the tilted **(c)** positions of the substrate at constant rotation speed. Several runs are also executed with a lower tilting rate (0.5°/s) and different rotation speed rates (0.5, 0.7, 1.5 rpm/s). It is found that the different tilting and rotation speed rates do not influence the results indicating that the experiments are not affected by dynamic phenomena. Advancing and receding contact angles are measured using the liquid injection/withdrawal procedure for the specific solid-liquid combination (i.e. glass-water).

Initially, droplets of all the examined volumes are tested under centrifugal forces alone to determine the rotating speeds corresponding to the onset of spreading and sliding. A rotation speed between these two thresholds is chosen to perform the experiments, where droplet elongation is noticeable but no sliding is detected. Next, the corresponding maximum tilting angle required to reach a symmetric droplet side profile is found by extensive experimentation for all the examined droplet volumes. The rotation speed and the maximum tilting angle used in the oscillation experiments are shown in Table 1.

The tangential, a_T, and normal acceleration, a_N, applied to the droplet are calculated by Eqs. 1a and 1b, respectively.

$$a_T = r \bullet \omega^2 \bullet \cos\alpha - g \bullet \sin\alpha \quad (1a)$$

Table 1
Pairs of rotation speed (*RS*, rpm) / tilting angle (α, °) applied during tilting oscillation experiments for the three different droplet volumes.

Volume (μL)	Rotation speed, *RS* (rpm)	Tilting angle, α (°)
10	64	38
20	55	31
30	45	23

$$a_N = r \bullet \omega^2 \bullet \sin\alpha + g \bullet \cos\alpha \quad (1b)$$

where ω is the angular speed derived as follows from the experimental rotation speed ($\omega = 2\pi \cdot f$, $f = RS/60$), r is the distance from the rotation axis to the droplet center (r = 25 cm for zero tilting) and α is the tilting angle of the substrate with respect to the horizontal orientation.

The acceleration applied to the tangential and normal directions can be expressed in normalized form as in Eqs. 2a and 2b using the definition of Bond numbers:

$$Bo_T = \frac{\rho \bullet L^2 \bullet a_T}{\sigma} \quad (2a)$$

$$Bo_N = \frac{\rho \bullet L^2 \bullet a_N}{\sigma} \quad (2b)$$

where ρ is the liquid density, L is a reference length (the value 1 mm is used here - its choice is explained in the theoretical section) and σ is the liquid surface tension.

During the tilting oscillations experiments, tangential and normal Bond numbers vary as presented in Fig. 2. The tangential Bond number acquires its maximum at zero tilting angle. The tangential force decreases as the tilting angle increases. The normal component of centrifugal and gravitational forces (c_N and g_N) acts in the same direction (Fig. 1). Therefore, the normal Bond number attains its maximum value at maximum tilting and its minimum value at zero tilting.

2.2. Approaching the SSP curve in three or six steps

This procedure is applied to droplets of 10 and 30 μL. The experiment begins with the selection of an initial rotation speed or an initial tilting angle lying between the corresponding spreading and sliding thresholds for the specific droplet volume. Then the tilting angle or the rotation speed is respectively adjusted to achieve a symmetric droplet side profile. Finally, the rotation speed and the tilting angle are successively varied, using three or six steps, in order to follow a path of symmetric side profiles. There are two different paths of this type: the first is performed increasing first the rotation speed and then the tilting angle and the second follows the opposite order (i.e. increasing first the tilting angle and then the rotating speed). The location of the successive experiments on the rotation speed-tilting angle plane for the two paths are shown in Fig. 3 for the three-step procedure and in Fig. 4 for the six-step procedure. The width of the rotation steps, except the first step, is 10 rpm and 5 rpm for the three-step and six-step experiments, respectively.

3. Results

This section presents separately the experimental results obtained during i) tilting oscillations procedure; and ii) trailing the symmetric side profile (SSP) curve in three and six steps following the two possible paths mentioned above.

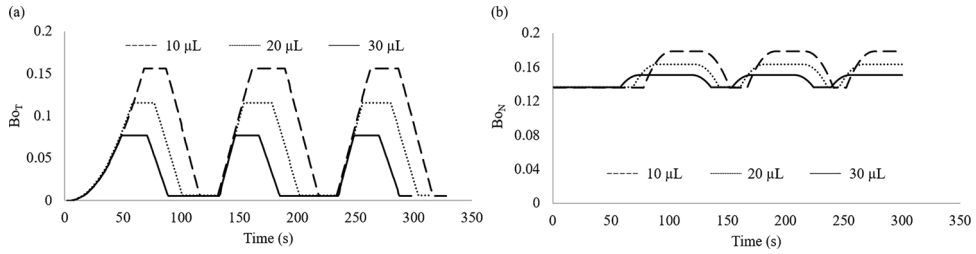

Fig. 2. Tangential (Bo_T) and normal (Bo_N) Bond numbers as a function of time during tilting oscillations at constant rotation speed for 10 (dashed), 20 (dotted) and 30 (solid) µL droplets.

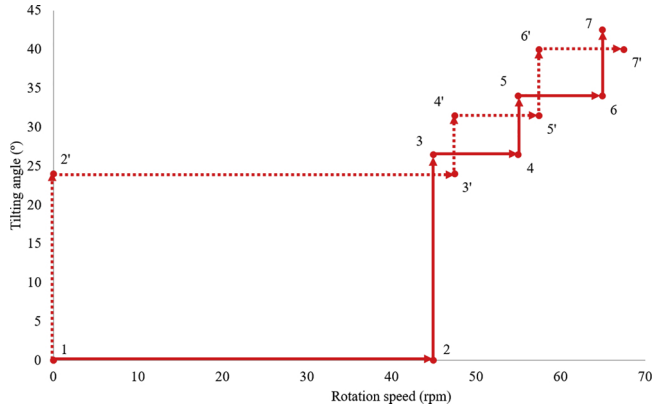

Fig. 3. SSP curve trailed in three steps through two different paths. The lines represent the path followed when an initial increase is applied to rotation speed (solid line), as compared to an initial increase of the tilting angle (dotted line).

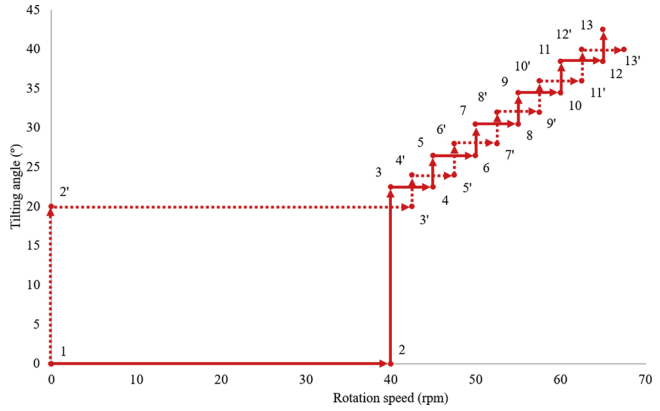

Fig. 4. SSP curve trailed in six steps through two different paths. The lines represent the path followed when an initial increase is applied to rotation speed (solid line), as compared to an initial increase of the tilting angle (dotted line).

3.1. Tilting oscillations procedure

The selected rotation speeds (*RS*) are 64, 55 and 45 rpm for 10, 20 and 30 µL droplet volume, respectively (see Table 1). After this maximum *RS* value is reached, the rotation speed is kept constant until the end of the experiment. The tilting angle of the substrate necessary to create a symmetric side profile for 10, 20 and 30 µL droplets is 38, 31 and 23°, respectively. For each of the droplet volumes, front and rear contact angles are measured and the evolution of the droplet side contour shape for the different operation parameters (*RS*, α) is investigated.

The droplet is, in all cases, initially axisymmetric at point **1** (panels from (a) to (c) of Fig. 5) when front (θ_F) and rear (θ_R) contact angles coincide at 55 ± 2°. Afterwards, the rotation speed is increased causing droplet deformation and spreading (point **2**). During spreading, the droplet front edge attains the advancing contact angle with the substrate ($\theta_F = \theta_A$). Dynamic contact angles (advancing and receding) in the quasi-steady limit (which is the case here as it will be discussed in the next section) depend only on the liquid-solid pair, and thus they are equal for the three different droplet volumes with a 2° margin of experimental error ($\theta_A = 60 \pm 2°$) (Fig. 5). From point **1** to **2** the droplet elongates in the direction of the centrifugal force. This process is irreversible, thus contact angles for the subsequent symmetric (side profile symmetry) positions (**3** and **5**) converge to a value that is 10° lower than the initial contact angle (for positions **3** and **5**, $\theta_F = \theta_R = 45 \pm 2°$). When the tilting angle (α) is increased to the value where c_T and g_T compensate each other, the droplet has a non-symmetric shape (its basis is no longer circular so even in the absence of tangential force θ_F and θ_R are not the same). A residual tangential force in the direction that created the elongation leads to $\theta_R = \theta_F$ (position **3**). In the subsequent oscillations the droplet shape alternates from symmetric to non-symmetric (zero tilting) without varying its contact area with the solid.

The droplet shape is analyzed from side and top views. The evaluation of the side profiles during oscillations reveals a bigger deformation in the first increase of the rotation (point **1** to **2**) compared to the subsequent deformations (points **3** to **4** and points **5** to **6**) for all droplet volumes. In addition, the deformation due to the oscillations is larger for the 30 µL droplet. Periodic variation of the applied force field appears to create periodic variation of the droplet shape. This means that in case of a constant contact line (contact angles being always between advancing and receding ones) any deformation induced to the droplet by an external force field is reversible.

The evolution of the droplets shape from above (i.e. top-view) is also evaluated. The droplets spread due to the rotation speed increasing from point **1** (initial shape) to point **2** (elongated shape). After this step, they keep the same top-view shape until the end of the experiment (from point **2** to **6**). In other words, the analysis of droplets' top-view contours does not reveal any spreading or shape changes from point **2** to **6**. Fig. 6 represents top-view images of the droplet initial shape (upper row) and elongated shape (lower row) for the three different droplet volumes under study.

The initial axisymmetric shape of the droplet observed from above can be immediately approximated with a circle (Fig. 6, upper row) [19]. Nevertheless, when forces are applied, and the droplet elongates at one edge (without sliding of the droplet), the contour no longer matches a circular shape. (Fig. 6, lower row). Several options have been proposed to approximate the contour of a droplet at the state of incipient motion such as 2 circle-arcs connected by parallel sides [20], [21], 2 ellipses sharing the minor axis [22] or just one ellipse [23]. In the current case, the best approximation combines a circle and an ellipse sharing the minor axis [24] as this fits the droplet contours very accurately. The dimensions of the circles and ellipses are presented in Table 2.

A 3D reconstruction of the droplet shape is obtained by elaborating in the combination of side and top droplet contours as explained in [17]. In Fig. 7, an example of the computed 3D shape for three different volumes at maximum spreading (position 2 in the Fig. 5) is presented.

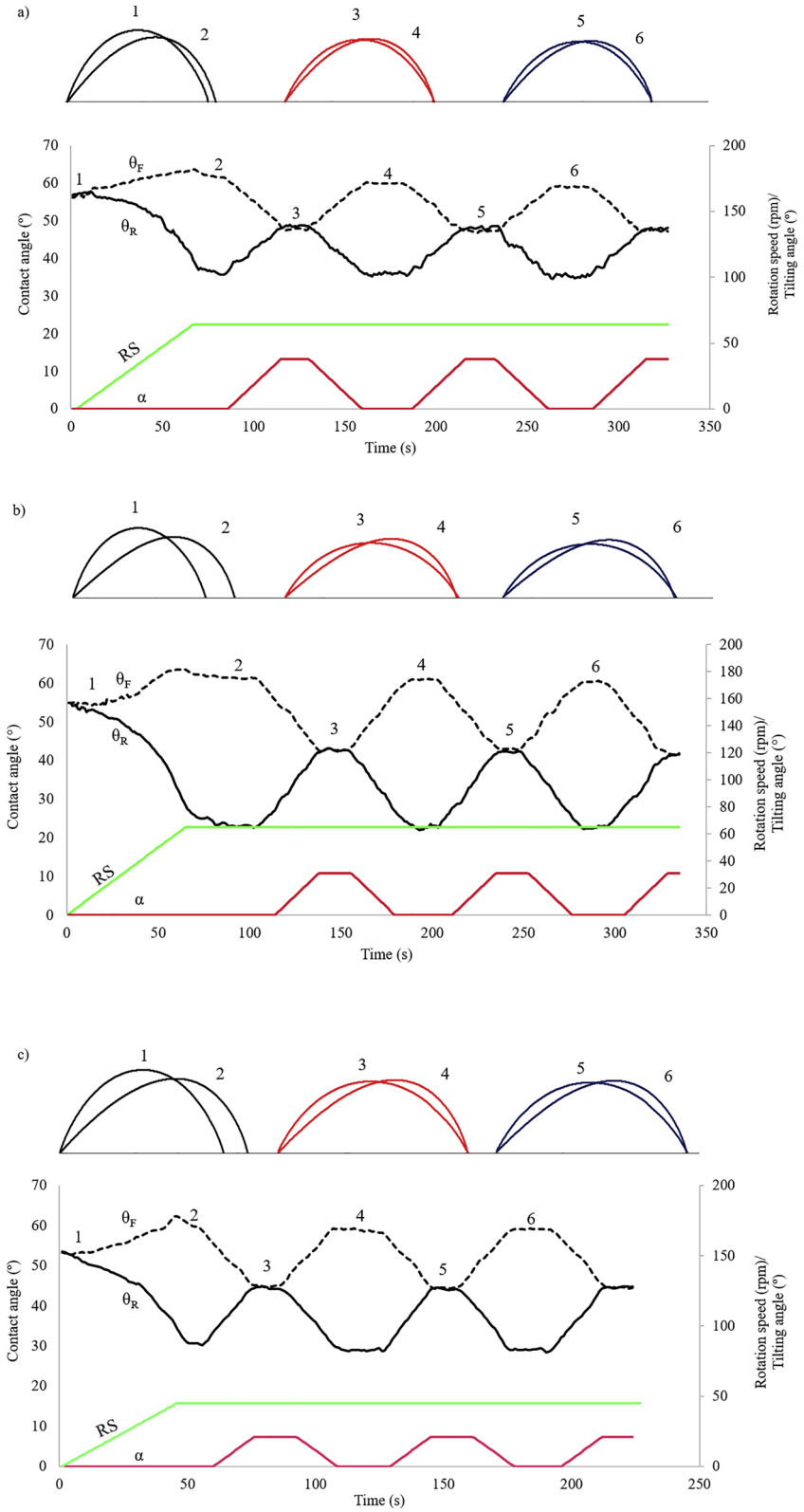

Fig. 5. Evolution of a droplet's side profile during three oscillations (1–2, 3–4 and 5–6) for droplet volume of 10 (a), 20 (b) and 30 (c) µl. Lines at the top represent the evolution of the front (θ_F, dashed) and rear (θ_R, solid) contact angles. Lines at the bottom depict the current value for rotation speed, *RS*, and tilting angle, α.

3.2. Trailing the SSP curves in three and six steps

As explained above, the SSP curve is trailed by increasing in small steps alternatively the rotation speed (*RS*) and the tilting angle (α). The experiments are performed for 10 and 30 µL droplets following two different paths: by initial increasing of a) the rotation speed; and b) the tilting angle.

The evolution of front and rear contact angles with time and operation parameters (*RS* and α) is presented for both the three-step (Fig. 8) and the six-step (Fig. 9) procedures. In Fig. 8, droplets of 10 µL

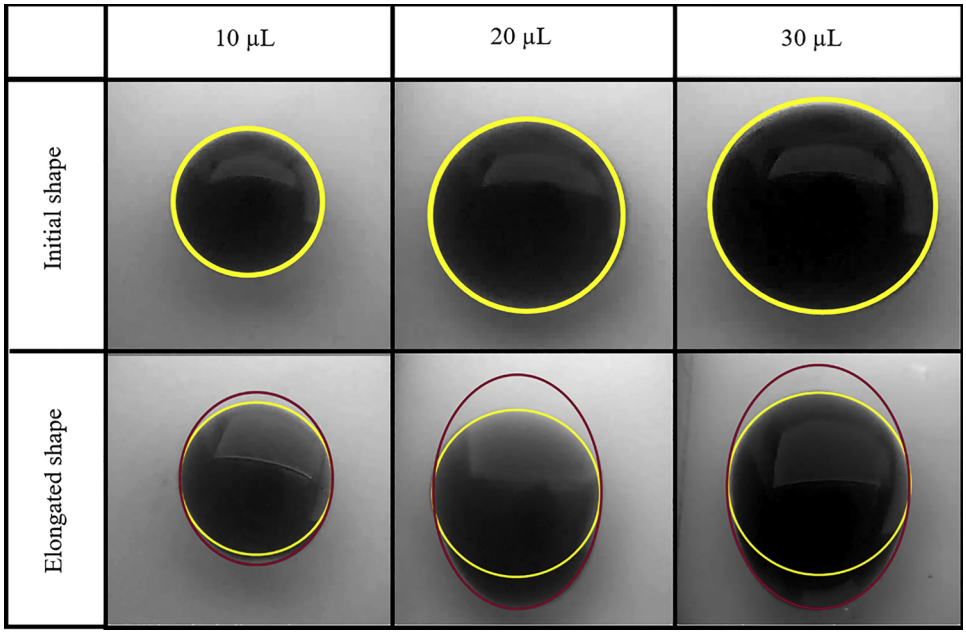

Fig. 6. Droplet's top-view images of 10, 20 and 30 μL volume at two different stages: initial shape (top raw) and elongated shape (bottom raw). The shapes are fitted using a circle (yellow line) and an ellipse (red line). (For interpretation of the references to colour in this figure legend, the reader is referred to the web version of this article).

Table 2
Dimensions of the circles and ellipses used to fit the top-view droplet contour for three different droplet volumes for initial and elongated shapes in tilting oscillation experiments.

Volume (μL)	Initial shape	Elongated shape			
	Circle diameter (mm)	Circle diameter (mm)	Ellipse short diameter (mm)	Ellipse long diameter (mm)	Total length (mm)
10	4.10	4.10	4.10	4.65	4.36
20	5.42	5.42	5.42	7.58	6.50
30	6.43	6.43	6.43	9.00	7.50

and 30 μL are explored during the three-step procedure, performing initial increase of the rotation speed (Fig. 8**a** and **c**) and initial increase of the tilting angle (Fig. 8**b** and **d**). The droplet spreads from point **1** to **2** (**2′**) and, thus the front contact angle (θ_F) reaches the value of the advancing contact angle in all cases (60 ± 2°). From point **2** (**2′**) to **7**, the droplet side profile alternates from a symmetric to a non-symmetric shape with the front and rear contact angles converging and diverging, respectively. As with the variation of contact angles in the tilting oscillations procedure, also here the contact angles that the droplet attains in the subsequent axisymmetric points (**3**, **5** and **7**) are lower than the initial contact angle due to the initial spreading stage. Deviations from axisymmetry, measured as the difference between front and rear contact angles ($\theta_F - \theta_R$), are equal (within experimental accuracy) for a particular droplet volume (after of course the initial spreading), independently of the path followed (initial increase either of rotation speed or tilting angle) comparing Figs. 8**a** and **b**; **c** and **d**. This deviation is about 5° and 10° for the 10 and 30 μL droplets, respectively.

The respective contact angle evolution for the six-step procedure is displayed in Fig. 9 for both droplet volumes and both experimental paths. In this case, the steps performed are half-wide (5 rpm wide as compared to the 10 rpm for the three-step procedure) and therefore, deviations from axisymmetry are smaller than for the three-step procedure (Fig. 8). These deviations are equal along the steps and independent of the followed path (Fig. 9**a** and **b**; **c** and **d**). The deviations are larger for the larger droplet volume (Fig. 9**a** and **c**; **b** and **d**) as in the previous case.

As with the tilting oscillations procedure, the droplet side profile evolution is evaluated for trailing the SSP curve in three and six steps. As shown in Fig. 10, for a 30 μL droplet, the rear edge stays pinned to the (0, 0) coordinate along the whole experiment (from point **1** to **6**). By contrast, the front edge advances during the first step (from point **1** to point **2**), and then stays stable through the two subsequent steps (from point **3** to point **4**, and from point **5** to point **6**). In other words, spreading occurs only in the first step while during the second and third steps the position of the edges is pinned, and the contact angles vary, making the droplet shape to change from symmetric (points **3** and **5**) to non-symmetric (**4** and **6**). The same holds for the six-step procedure in which droplet spreading occurs in the first step from point **1** to **2** with the advancement of the front edge. However, during subsequent steps (point **2** to **12**), both edges are pinned to the same location. Fig. 11 depicts droplet side profiles for a 10 μL droplet during the six-step procedure following the path of initial increase of rotation speed.

Finally, the parameters of the fitting circles and ellipses for the

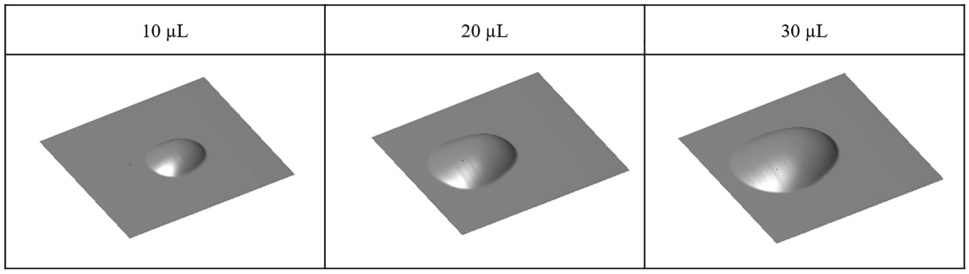

Fig. 7. Droplet's 3D reconstruction based on the combination of side and top contours at maximum elongated stage (Point 2, Fig. 5) for three volumes (10, 20 and 30 μL).

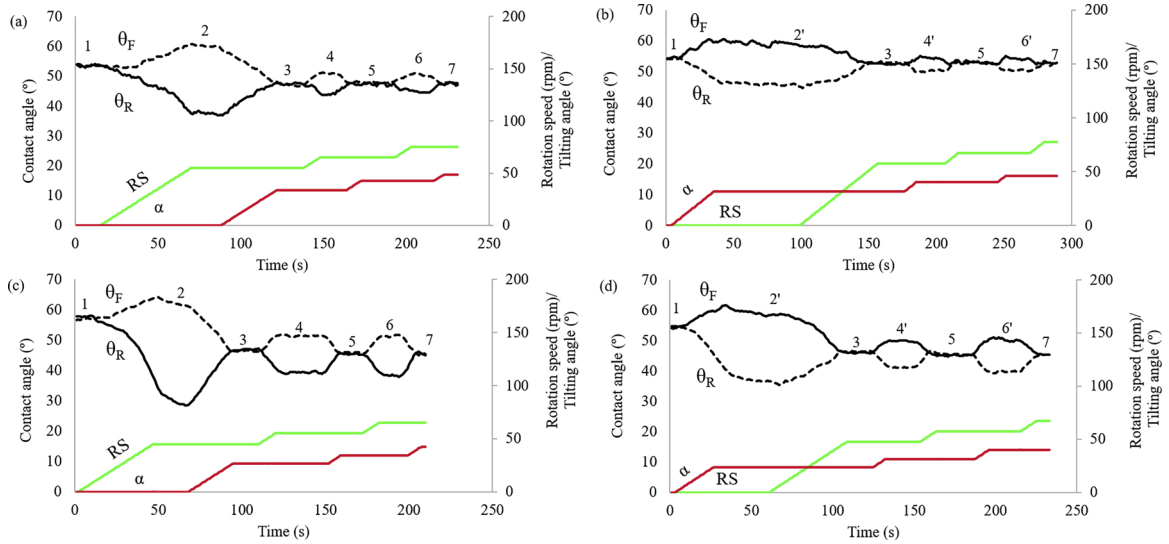

Fig. 8. Front (θ_F, dashed) and rear (θ_R, solid) contact angle evolution versus time for 10 μL (a and b) and 30 μL (c and d) droplets according to the three-step procedure to follow the SSP curve. Plots depict the evolution of contact angle when the initial increase is applied to the rotation speed (a and c) or to the tilting angle (b and d). Numbers from 1 to 7 correspond to positions on the SSP curves in Fig. 3.

evolution of the droplet top-view are presented in Table 3. As for the tilting oscillation experiments, the droplet contact line spreads with the first increase of the force and stays constant during subsequent steps when observed from above. Results are presented for a 30 μL droplet for a three step procedure performing initial increase of a) the rotation speed; and b) the tilting angle. The experimental results follow the wetting/spreading theory qualitatively. That is, the droplet contact line remains constant as the contact angle limits (advancing and receding) are not exceeded. Furthermore, any shape deformation of the droplet of constant basis is reversible. Although it appears trivial, there are no experiments in literature further to the classical ones of an increasing tangential force. So, aspects such as the completely periodical response to periodic external forcing, as far as the contact angles remains between the advancing/receding ones, is considered to be an important information validating qualitatively the wetting theory. The quantitative information comes latter by showing that the experimental profiles almost coincide to those predicted by Young-Laplace equation. The findings are also a confirmation of the quasisteady nature of the present experiments.

4. Theoretical analysis and discussion

4.1. Model development

The current experimental data are analyzed on the basis of quasi-static droplet shape evolution. Moreover, the focus of the analysis is restricted on shape evolution under constant droplet contact line while varying the applied force. The quasi-static assumption is justified in the following way: Regarding droplet hydrodynamics characteristic time, it can be shown that it is of the order of few seconds for the droplet size of the present experiments (computed as the squared characteristic length divided by the liquid kinematic viscosity; it is noted that the droplet height is the relevant characteristic length). Considering the marginal droplet shape deformation in this time scale, shown in the droplet

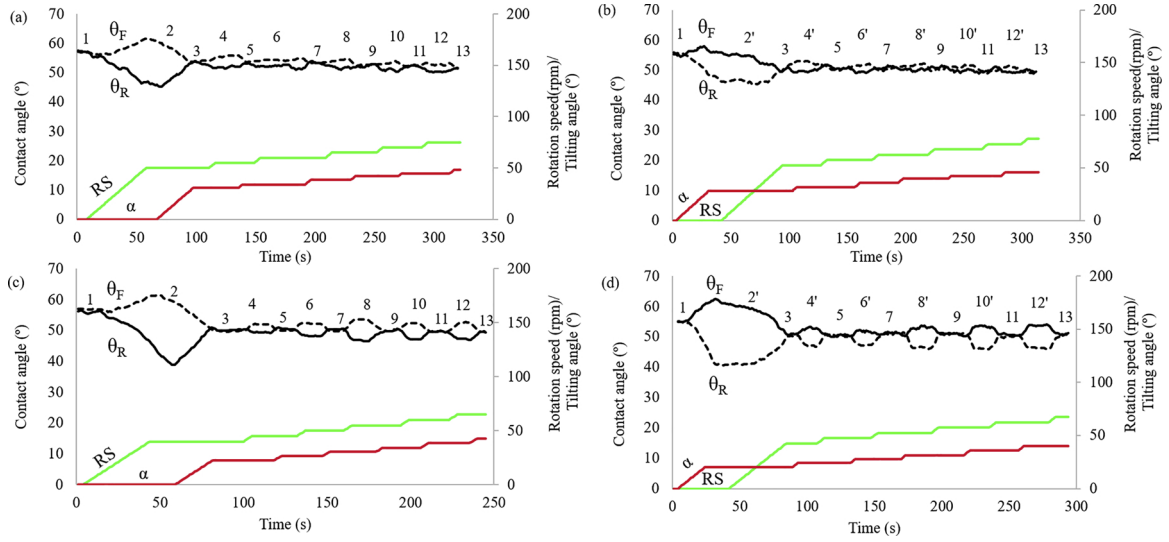

Fig. 9. Front (θ_F, dashed) and rear (θ_R, solid) contact angle evolution versus time for 10 μL (a and b) and 30 μL (c and d) according to the six-step procedure to follow the SSP curve. Plots depict the evolution of the contact angle when the initial increase is applied to the rotation speed (a and c) or to the tilting angle (b and d). Numbers from 1 to 13 correspond to position on the SSP curves in Fig. 4.

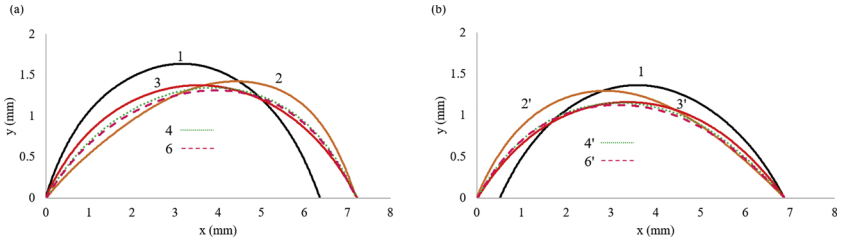

Fig. 10. Side profile evolution for a 30 µL droplet according to the three-step procedure to follow the SSP curve with initial increase of a) rotation speed and b) tilting angle. Curves 1 and 3 depict symmetric profiles whereas 2, 4, and 6 depict non-symmetric profiles. Intermediate symmetric profile 5 is not plotted as it is considered equal to profile 3.

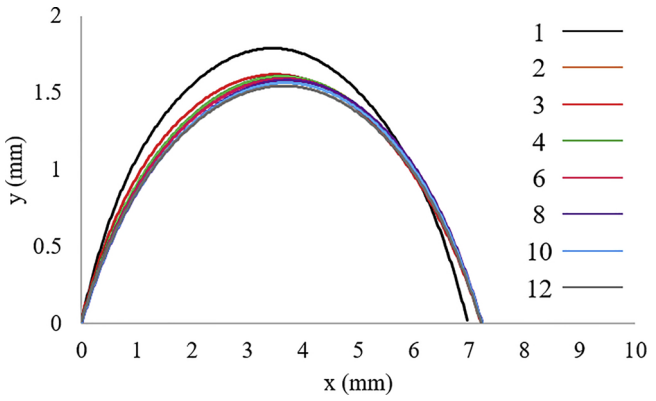

Fig. 11. Side profile evolution for a 10 µL droplet according to the six-step procedure to follow the SSP curve with initial increase of the rotation speed. Curves 1 and 3 depict symmetric profiles whereas 2, 4, 6, 8, 10 and 12 depict non-symmetric profiles. Intermediate symmetric profiles 5, 7, 9 and 11 are not plotted as they are indistinguishable from profile 3.

Table 3
Dimensions of the circles and ellipses used to fit the top-view droplet contour for a 30 µL droplet for initial symmetrical and elongated shapes when following the SSP curve in three steps following two different paths: a) initial increase of rotation speed, b) initial increase of tilting angle.

	3 steps			
	a)		b)	
Shape	Initial	Elongated	Initial	Elongated
Circle diameter (mm)	6.43	6.43	6.37	6.37
Ellipse long axis (mm)	–	8.11	–	7.22
Ellipse short axis (mm)	–	6.43	–	6.37

profiles of the previous section, it appears that the quasi steady approximation is valid. Another characteristic time is associated with the contact line motion but, as explained already, such a motion is not analyzed here. The droplet shape in the quasi-static limit is described by the Young-Laplace equation which is the balance between surface and bulk forces in the droplet. In this respect, the complete three dimensional non-linear Young-Laplace equation is solved. Its solution requires numerical techniques, but it is physically accurate since it describes the actual shape that the droplet attains for a specified contact line.

The problem has a not intrinsic characteristic length (in general the droplet length is unknown) so usually the capillary length is used for non-dimensionalization [25]. We found more convenient to use as characteristic length a size scale simply representative of the droplet size instead of using the explicit capillary length or droplet dimension. This choice in the present work is L = 1 mm as it has been already referred. The major advantage of using this characteristic length in the definition of Bond number (Eq. 2) is that it reflects solely the external forcing field and it is not related to the specific droplet size. On the other hand, the normalized droplet volume does not depend on acceleration field or on type of the liquid. In what follows all the length variables (x,y,f) are normalized with L and the droplet volume is normalized with L^3.

Let us denote as x, y a system of Cartesian coordinates on the substrate. The contact line is described by the closed curve F(x,y) = 0. Let C be the domain enclosed by the curve F = 0. The equation that describes the shape of the droplet f(x,y) for a tangential force in the positive x direction and for contact angles smaller than 90° (the variables f, x, y are normalized by the characteristic length L and the variable V is normalized by L^3) is [25]:

$$-\left(1+\left(\frac{\partial f}{\partial y}\right)^2\right)\frac{\partial^2 f}{\partial x^2}+2\frac{\partial f}{\partial x}\frac{\partial f}{\partial y}\frac{\partial^2 f}{\partial x\partial y}-\left(1+\left(\frac{\partial f}{\partial x}\right)^2\right)\frac{\partial^2 f}{\partial y^2}$$
$$=\left(1+\left(\frac{\partial f}{\partial x}\right)^2+\left(\frac{\partial f}{\partial y}\right)^2\right)^{\frac{3}{2}}(G-Bo_N f+ Bo_T x) \quad (3)$$

The boundary condition for the solution of the above equation is

$$f = 0 \text{ on } F(x,y) = 0 \quad (4)$$

The parameter G is a dummy variable associated with the pressure in the droplet and it must be found from the constraint of droplet volume:

$$V=\iint_C f(x, y)dxdy \quad (5)$$

where V is the droplet volume (real volume in the 3D problem). Eq. (3) must be solved numerically. An unstructured triangular grid is defined on the domain C. Then a finite element discretization (with quadratic elements) is applied to the governing equation. The resulting non-linear system of algebraic equations is solved by the Newton-Raphson procedure. In this way, the profile f can be computed for an assumed value of G. The corresponding volume $V_g(G)$ is computed by numerical integration of Eq (5). In order to find the value of G that corresponds to the actual droplet volume V the equation $V_g(G) = V$ is solved using again (as an outer iteration loop) the Newton Raphson method. It is noted that the solution of this equation includes repeated calls to the finite element solver. The shape of the contact line uniquely determines the distribution of contact angles along the contact line through the solution of the governing Young-Laplace equation. We prefer to keep the term" contact angle" instead of the "apparent contact angle" since the latter is usually employed to discriminate microscopic (roughness scale) from droplet scale phenomena. The distribution of contact angles here refers to the droplet scale.

It must be argued that the acceleration field produced by the rotation is not uniform as assumed above but in fact varies along the droplet. This problem has been studied in [16] and it was shown that the error in the resulting droplet shape due to the assumption of uniform acceleration depends on the ratio droplet length/distance of droplet from rotation axis, i.e. β/R. For the values of this ratio in the present experiments the assumption of uniform acceleration in the droplet is quite accurate. The uniform acceleration has to be computed at the center of the droplet. This might require an iterative procedure in terms of the unknown droplet length, but this is not necessary here because the length is known from the experiments.

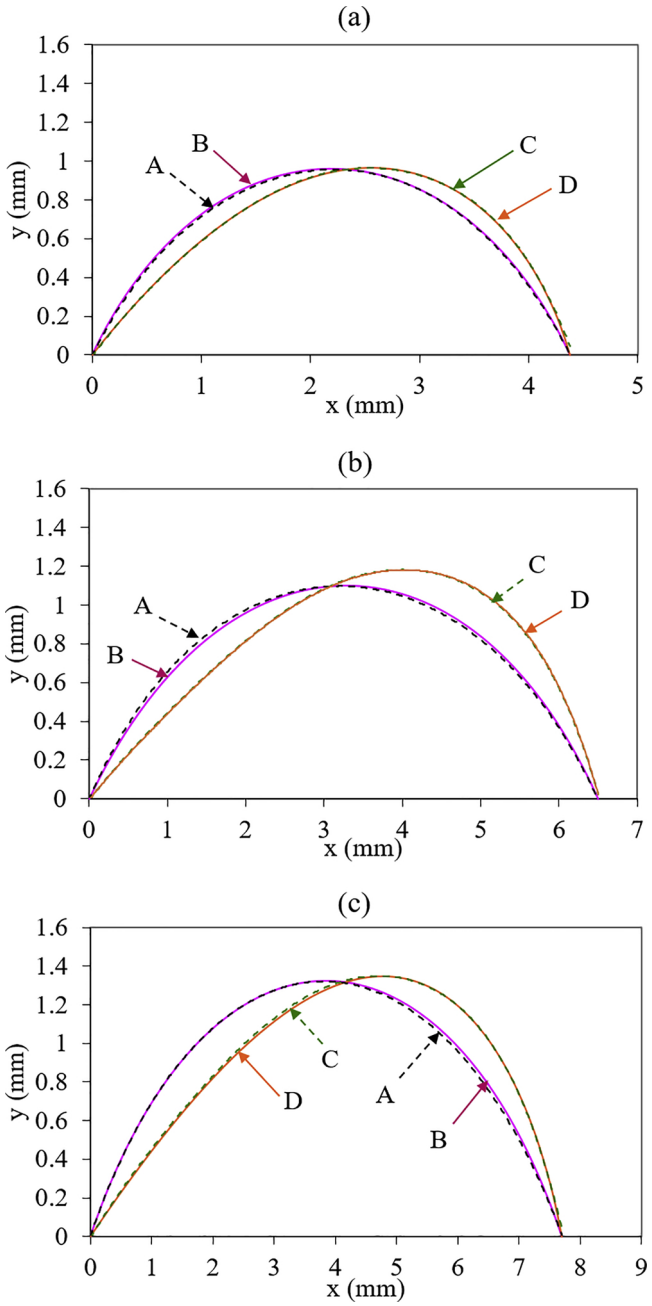

Fig. 12. Comparison between experimental and theoretical droplet side profiles for (a) 10 µl, (b) 20 µl and (c) 30 µl droplets at several positions during tilting oscillation experiments. Curves A: experimental position 3, B: theoretical position 3, C: experimental position 4, D: theoretical position 4. See positions 3 and 4 in Fig. 5.

4.2. Comparison with the experiments

For given experimental snapshots the Young Laplace equation is solved by considering the experimental droplet base profile and by matching the actual droplet volume. The 2D droplet profile at symmetry plane is extracted from the 3D computed droplet shape and is compared to the side experimental droplet profile. This comparison for droplets of 10, 20, 30 µL and for positions 3 and 4 (as denoted in Fig. 5) are presented in Fig. 12. It is evident that in all cases the deviation between experimental and theoretical profiles is in the limit of the image processing resolution. This confirms the quasi-steady nature of the droplet shape. It is interesting to note that the symmetry of the side profile is not achieved at zero tangential force. This is because the droplet base does not exhibit fore and aft symmetry, so the front and rear contact angles are different in the absence of tangential force.

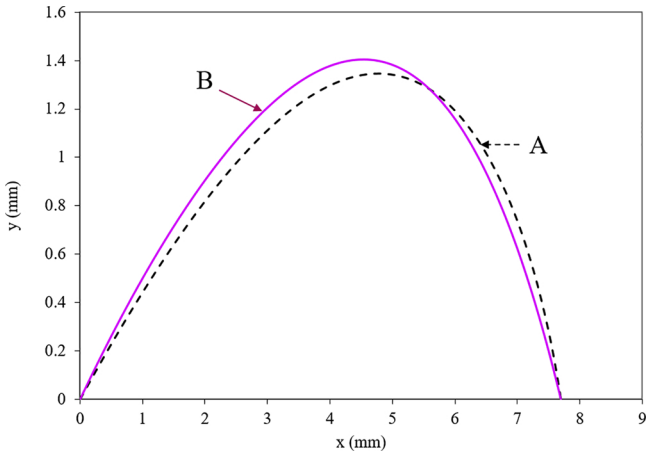

Fig. 13. Theoretical side profiles predicted by Young Laplace equation for 3D droplets. Droplet volume 30 µl, position 4 of tilting oscillation experiments in Fig. 5. Curves A: Complete equation, B: Exclusion of non-linear terms.

A question is raised if the linearization of the Young-Laplace equation for the droplet shapes arising in the present work is permissible. To get a better insight, the three-dimensional linearized Young-Laplace equation (i.e. Eq (3) with all the first order derivative terms equal to zero) is solved for the 30 µL droplet at position 4. The comparison between non-linear and linear approaches is shown in Fig. 13. It is evident that linearization leads to a significant underprediction of deformation under tangential force. Although the present droplets appear elongated, they are not thin enough to exclude nonlinearity and the complete Young-Laplace equation is needed for their description. The above findings suggest design guidelines for wetting applications considering quasisteady conditions and complex applied forces sequences. The basic tool must be the three dimensional Young-Laplace equation. However, the contact line shape cannot be determined by a fundamental theory and extensive experimental results like the present ones are needed.

5. Conclusions

This work presents innovative experiments on droplet shape evolution during application of complex, non-conventional, force scenarios using *Kerberos* device. In particular, experiments with tilting oscillations at constant speed of rotation as well as experiments with alternating small step changes in tilting and rotation in order to maintain symmetric droplet shapes are performed. The results appear to follow the behavior suggested by classical wetting theory. The experimental droplet profiles are compared with solutions of the linearized two-dimensional and of the non-linear three-dimensional Young-Laplace equation. The non-linear three-dimensional Young-Laplace equation can describe very well the experimental profiles confirming that they correspond to quasi-steady conditions. Linearization of the Young Laplace equation is not adequate to describe the droplet shapes of the present work.

Acknowledgements

This work was supported by Marie-Curie ITS “Complex wetting Phenomena, CoWet” (FP7-PEOPLE-2013-ITN, grant number 607861) and by MAP Project “Enhanced Condensers in Microgravity, ENCOM-3″ (European Space Agency, Contract No.: 4200020276) and was carried out under the umbrella of COST Action MP1305 “Flowing Matter”.

References

[1] S.J. Hong, C.C. Chang, T.H. Chou, Y.J. Sheng, H.K. Tsao, A drop pinned by a designed patch on a tilted superhydrophobic surface: mimicking desert beetle, J. Phys. Chem. C. 116 (2012) 26487–26495, https://doi.org/10.1021/jp310482y.

[2] Y.Y. Yan, N. Gao, W. Barthlott, Mimicking natural superhydrophobic surfaces and grasping the wetting process: a review on recent progress in preparing superhydrophobic surfaces, Adv. Colloid Interface Sci. 169 (2011) 80–105, https://doi.org/10.1016/j.cis.2011.08.005.

[3] J. Kim, M.W. Moon, K.R. Lee, L. Mahadevan, H.Y. Kim, Hydrodynamics of writing with ink, Phys. Rev. Lett. 107 (2011) 2–5, https://doi.org/10.1103/PhysRevLett.107.264501.

[4] S. Li, J. Huang, Z. Chen, G. Chen, Y. Lai, A review on special wettability textiles: theoretical models, fabrication technologies and multifunctional applications, J. Mater. Chem. A 5 (2017) 31–55, https://doi.org/10.1039/c6ta07984a.

[5] N.R. Morrow, Wettability and its effect on oil recovery, J. Pet. Technol. 42 (1990) 1476–1484.

[6] D. Brutin, V. Starov, Recent advances in droplet wetting and evaporation, Chem. Soc. Rev. 47 (2018) 558–585, https://doi.org/10.1039/c6cs00902f.

[7] G. Lu, X.D. Wang, Y.Y. Duan, A critical review of dynamic wetting by complex fluids: from Newtonian fluids to non-Newtonian fluids and nanofluids, Adv. Colloid Interface Sci. 236 (2016) 43–62, https://doi.org/10.1016/j.cis.2016.07.004.

[8] T.D. Blake, The physics of moving wetting lines, J. Colloid Interface Sci. 299 (2006) 1–13, https://doi.org/10.1016/j.jcis.2006.03.051.

[9] Y. Zhao, Y. Wang, Fundamentals and applications of electrowetting: a critical review, Rev. Adhesion Adhesives 1 (2013) 114–174, https://doi.org/10.7569/RAA.2013.097304 Abstract.

[10] T.D. Blake, J.C. Fernandez-Toledano, G. Doyen, J. de Coninck, Forced wetting and hydrodynamic assist, Phys. Fluids. 27 (2015), https://doi.org/10.1063/1.4934703.

[11] B.N.K. Adam, G. Jessop, Angles of contact and polarity of solid surfaces, J. Chem. Soc. 127 (1925) 1863–1868.

[12] C.W. Extrand, A.N. Gent, Retention of liquid drops by solid surfaces, J. Colloid Interface Sci. 138 (1990) 431–442, https://doi.org/10.1016/0021-9797(90)90225-D.

[13] R. Goodwin, D. Rice, S. Middleman, A model for the onset of motion of a sessile liquid drop on a rotating disk, J. Colloid Interface Sci. 125 (1988) 162–169, https://doi.org/10.1016/0021-9797(88)90065-3.

[14] A.M. Goula, T.D. Karapantsios, K.G. Adamopoulos, An advanced centrifugal technique to characterize the sticking properties of tomato pulp during drying, Dry. Technol. 25 (2007) 599–607, https://doi.org/10.1080/07373930701227151.

[15] R. Tadmor, P. Bahadur, A. Leh, H.E. N'Guessan, R. Jaini, L. Dang, Measurement of lateral adhesion forces at the interface between a liquid drop and a substrate, Phys. Rev. Lett. 103 (2009) 1–4, https://doi.org/10.1103/PhysRevLett.103.266101.

[16] S.P. Evgenidis, K. Kalić, M. Kostoglou, T.D. Karapantsios, Kerberos: a three camera headed centrifugal/tilting device for studying wetting/dewetting under the influence of controlled body forces, Colloids Surf A 521 (2017) 38–48, https://doi.org/10.1016/j.colsurfa.2016.07.079.

[17] I. Ríos-López, P. Karamaoynas, X. Zabulis, M. Kostoglou, T.D. Karapantsios, Image analysis of axisymmetric droplets in wetting experiments: A new tool for the study of 3D droplet geometry and droplet shape reconstruction, Colloids Surf A 553 (2018) 660–671, https://doi.org/10.1016/j.colsurfa.2018.05.098.

[18] I. Ríos-López, S. Evgenidis, M. Kostoglou, X. Zabulis, T.D. Karapantsios, Effect of initial droplet shape on the tangential force required for spreading and sliding along a solid Surface, Colloids Surf A 549 (2018) 164–173, https://doi.org/10.1016/j.colsurfa.2018.04.004.

[19] J.J. Bikerman, Sliding of drops from surfaces of different roughnesses, J. Colloid Sci. 5 (1950) 349–359, https://doi.org/10.1016/0095-8522(50)90059-6.

[20] C.G.L. Furmidge, Studies at phase interfaces. I. The sliding of liquid drops on solid surfaces and a theory for spray retention, J. Colloid Sci. 4 (1962) 309–324.

[21] E.B. Dussan, On the ability of drops or bubbles to stick to non-horizontal surfaces of solids, J. Fluid Mech. 151 (1985) 1–20, https://doi.org/10.1016/0305-0548(75)90015-5.

[22] M. Bouteau, S. Cantin, F. Benhabib, F. Perrot, Sliding behavior of liquid droplets on tilted Langmuir-Blodgett surfaces, J. Colloid Interface Sci. 317 (2008) 247–254, https://doi.org/10.1016/j.jcis.2007.09.042.

[23] A.I. ElSherbini, A.M. Jacobi, Liquid drops on vertical and inclined surfaces: I. An experimental study of drop geometry, J. Colloid Interface Sci. 273 (2004) 556–565, https://doi.org/10.1016/j.jcis.2003.12.067.

[24] M. Higashine, K. Katoh, T. Wakimoto, T. Azuma, Profiles of liquid droplets on solid plates in gravitational and centrifugal fields, Japanese Soc Exp Mech. 8 (2008) 49–54, https://doi.org/10.11395/jjsem.8.s49.

[25] C. Pozrikidis, Introduction to Theoretical and Computational Fluid Dynamics, Oxford University Press, USA, 2011.